This article has been accepted for publication in a future issue of this journal, but has not been fully edited. Content may change prior to final publication. Citation information: DOI 10.1109/JSEN.2018.2814839, IEEE Sensors Journal

Design, Modeling, and Validation of a Soft Magnetic 3-D Force Sensor

Anany Dwivedi, Anand Ramakrishnan, Aniketh Reddy, Kunal Patel, Selim Ozel, Cagdas D. Onal

***Abstract*—Recent advances in robotics promise a future where robots co-exist and collaborate with humans in unstructured environments, which will require frequent physical interactions where accurate tactile information will be crucial for performance and safety. This article describes the design, fabrication, modeling, and experimental validation of a soft-bodied tactile sensor that accurately measures the complete 3-D force vector for both normal and shear loading conditions. Our research considers the detection of changes in the magnetic field vector due to the motion of a miniature magnet in a soft substrate to measure normal and shear forces with high accuracy and bandwidth. The proposed sensor is a pyramid-shaped tactile unit with a tri-axis Hall element and a magnet embedded in a silicone rubber substrate. The non-linear mapping between the 3-D force vector and the Hall effect voltages is characterized by training a neural network. We validate the proposed soft force sensor over static and dynamic loading experiments and obtain a mean absolute error below 11.7 mN or 2.2% of the force range. These results were obtained for a soft force sensor prototype and loading conditions not included in the training process, indicating strong generalization of the model. To demonstrate its utility, the proposed sensor is used in a force-controlled pick-and-place experiment as a proof-of-concept case study.**

I. INTRODUCTION

Direct force and tactile sensing remains an open technical problem in robotics [1]–[3]. To address this problem, new sensing mechanisms and modeling approaches need to be developed to achieve compliant, safe, and aware interactions between robots, human users, and the environment. We observe three fundamental challenges that impede progress [4]. First, it is difficult to obtain a reliable sensing modality between external forces and a measurable change in a physical medium, without detrimental nonlinearities or other artifacts such as hysteresis or time delay. Second, modeling to obtain a reliable map between the external force and the measured physical change is challenging, especially for multi-dimensional measurements. Finally, scalability tends to be a challenge, to obtain useful spatial resolution over a surface, while avoiding crosstalk between sensing elements. This article adresses each challenge by presenting a magnetic sensing modality and neural network based modeling of a small tri-axial soft sensing element.

This material is based upon work supported by the National Science Foundation (NSF) under Grant No. CNS-1544636. Any opinions, findings, and conclusions or recommendations expressed in this material are those of the authors and do not necessarily reflect the views of the NSF.

The authors are with the WPI Soft Robotics Laboratory, Mechanical Engineering Department and Robotics Engineering Program, Worcester Polytechnic Institute, MA 01609, USA. All correspondence should be addressed to Cagdas Onal cdonal@wpi.edu

Anany Dwivedi and Anand Ramakrishnan contributed equally to this work.

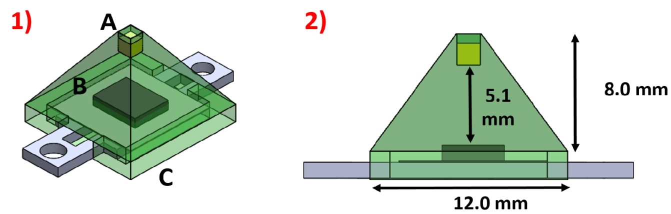

Fig. 1: 1) Design of the proposed tri-axial soft force sensor utilizes a miniature magnet (A), Hall Effect IC (B), and a circuit layer on an acrylic sheet (C), embedded in a pyramid shaped silicone rubber substrate. 2) The sensor prototype is 8 mm tall with an 12 mm wide square base.

In terms of sensing medium, tactile sensing literature may be classified into: 1) stimuli responsive and/or composite materials that mainly employ resistive or capacitive measurements, and 2) using embedded discrete electronic components or other physical quantities such as optical or magnetic signals within the sensor body. Resistive sensing has been a popular method, although it may suffer from dynamic artifacts [5]–[8]. In [9], Wood et al. uses a conductive fluid (eGaIn) placed in channels created on a soft matrix to measure applied forces. These are multi-axis force sensors and can measure forces in normal and shear directions. But fabrication using eGaIn involves a number of challenges which are discussed in [10]. Alternatively, [11] measures pressure (or force) in the normal direction by the change in capacitance between two PDMS layers filled with carbon nanotubes. A similar measurement idea is realized via conductive textiles in [12]. In [13] the authors present pressure and position sensors made of conductive elastomers co-printed into a soft actuator in a single process without assembly. These sensors are capable of providing feedback because of their innovative design and the piezoresistive effect of conductive elastomers.

On the other hand, in [14], a commercially available barometric IC is embedded in a soft elastomer, to perform as a 1-D tactile sensor to measure normal forces. Yi et al. [15] presents a tactile sensor using optical fiber Bragg grating based on phase modulation of the optical source to determine the forces applied on the sensor. In [8], Sohgawa et al. propose a resistive tactile sensor using piezo-resistive cantilevers embedded in a soft matrix. It is important to note that these existing solutions suffer from various inherent challenges such as a lack of 3-D force sensing capability, relatively complex fabrication and signal processing circuitry, or hysteresis and time delay.

Regardless of the sensing medium, modeling and obtaining a reliable mapping between the force and the measured physi-

This article has been accepted for publication in a future issue of this journal, but has not been fully edited. Content may change prior to final publication. Citation information: DOI 10.1109/JSEN.2018.2814839, IEEE Sensors Journal

cal change is crucial and challenging, especially for multi-axis force sensing. The work in [16] employs multiphysical finite element analysis (FEA) to describe the behavior of a dome-shaped magnetic tactile sensor. Using FEA models are useful but in a multiphysics environment small errors and initial settings reflect heavily during the actual experimental testing of the sensors and since elastomers (e.g. Ecoflex 0030) are known to be highly nonlinear, FEA modeling is not straightforward. In addition, such models are usually not applicable for real-time computation.

In [9], authors approximate the sensor's resistance change response as linear and create a calibration matrix using least mean squares method. A similar approach was taken in [17], where a linear regression model was employed to find the relationship between force applied and the corresponding change in voltage. The linearity approximation makes these models simple enough to calculate the force mapping in real-time, but they are highly simplistic and thus, prone to errors. Response reliability is also important. In [11], authors mention carbon nanotubes not being aligned after repetitive loading. The resulting hysteresis can be reduced by depositing carbon nanotubes at a pre-stretched state, which may increase complexity and repeatability issues. These limitations motivated us to consider approaches that use machine learning as a method for estimating the complex relationship between the applied force and the measured change in the magnetic field vector in the proposed sensor to offer both accurate modeling and real-time computation for the nonlinear sensory mapping.

Using an embedded miniature magnet and flexible electronics in a soft substrate, we have previously shown that sensing local changes in magnetic field is suitable for accurate and high-speed measurements on the curvature of a flexible bending body [18]. In previous research, our objective was to obtain curvature measurement from soft silicone rubber segments for a specific type of bending soft actuator utilized in a snake robot [19]. This article employs similar design principles to force/contact measurements on a soft deformable substrate and in a small form factor.

Hall effect based sensors have gained prominence recently [16], [20]–[24]. In [22], Tomo et al. presents a soft sensor which utilizes a magnet for detecting forces in multiple axes. 16 Hall-effect ICs are used in total for one sensor module, hence adding to the complexity of the design. In this work, we present accurate force measurement results using a single IC with a magnet on top. We also do not need any explicit noise filter thus enabling our sensor to retain a faster response.

Our sensor design utilizes a 3-axis Hall effect sensor IC and a small magnet placed over it at a defined location, embedded inside a soft elastomer substrate. This gives the composite mechatronic structure the compliance required for force sensing. A 3-D model is shown in Figure 1. Any force applied on the soft matrix produces a deformation on it, which changes the position of the embedded magnet and this in turn causes changes in the magnetic flux values around the Hall element. This measured change has a non-trivial relation to the force applied on the sensor module.

We introduce two main novel contributions with this work. We use a neural network to calibrate the force sensor in 3-D and demonstrate its generalization ability to other materials and loading conditions. We show that the network is able to learn to respond to a large range of force directions whereas only small number of training forces are applied at pre-determined directions. We also show that the same network can be used with sensor prototypes that were not in the training set. This means that the network is able to overcome minor manufacturing differences and it can be used to scale up the sensing resolution without scaling up the calibration efforts. Recently the usage of machine learning has seen great interest for capturing complex relationships between the input space (forces) and the output space (the sensor measurement) [25]. In [22], fully connected neural networks (FCNs) are explored for characterization. However, the results show that the network is not able to generalize beyond the training conditions. Here, we present FCNs based on the Net2Net initialization technique [26], which provides better regularization of the network. We show that our network is able to generalize very well in Section III.

The second novelty is the pyramid shape. One of the main factors that affect the dependability of a tactile magnetic sensing element is its shape [27]. The shape of the contact surface that tapers to a point helps in restricting and channeling the movement of the magnet inside the soft matrix. In [16] we see a dome-shaped magnetic soft sensor with the magnet immediately below the dome which helps in obtaining a highly accurate model of the sensor. In [22] the shape of the soft matrix is a cuboid and the magnet is placed over the Hall element. A considerable problem with these designs are that the applied force may cause rotation of the magnet about its own axis in unmodeled ways, thus requiring additional calibration data and also reducing measurement dependability. In this work, we utilize the shape of a pyramid with the magnet embedded within the pyramid (as close to the centroid as practically possible). The advantage of this shape is that off-center forces acting on the sensor would tend to act about the centroid of the sensor and thus the tendency of rotation of the magnet about its own axis is reduced, greatly improving reliability.

This article is organized as follows: In Section II we discuss the design and manufacturing methods for the proposed soft 3-D force sensor. We include detailed information on electronics and fabrication process. In Section III we discuss in detail how data is collected for characterization and how it is used to map the function space of the sensor by a Neural Network. In Section IV, we discuss the results for the dynamic response test on the sensor and also present a use case application of the force sensor by performing force control on the fingers of a Jaco arm. Finally, we conclude the paper and discuss our future plans in Section V.

II. Sensor Design and Fabrication

The proposed 3-D force sensor utilizes tri-axial measurement of the magnetic field vector created by a miniature permanent magnet embedded in a pyramid shaped silicone rubber body as shown in Fig. 1. Magnetic fields are measured locally using a Hall element on an embedded custom

This article has been accepted for publication in a future issue of this journal, but has not been fully edited. Content may change prior to final publication. Citation information: DOI 10.1109/JSEN.2018.2814839, IEEE Sensors Journal

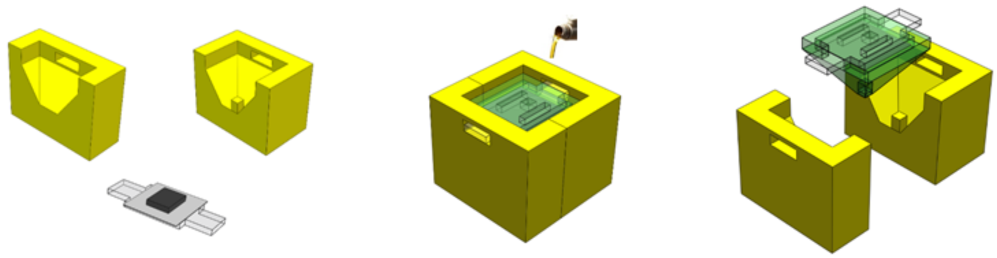

a) 3D printed molds required for fabricating the sensor are shown in yellow (top). A custom flexible PCB is bonded to an acrylic carrier (bottom).

b) The molds are clamped together with the acrylic circuit carrier and liquid silicone rubber precursor is introduced.

c) Cured silicone rubber sensor body is demolded with a cavity for the magnet.

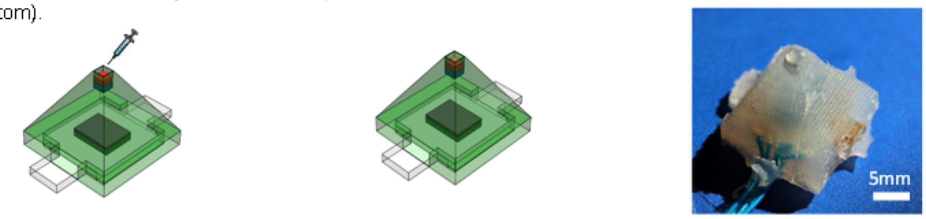

d) Magnet is placed in the cavity and liquid silicone rubber is injected to seal it in place.

e) Cured and finished force sensor module CAD model.

f) Actual force sensor prototype.

Fig. 2: Manufacturing process of the proposed tri-axial soft force sensor

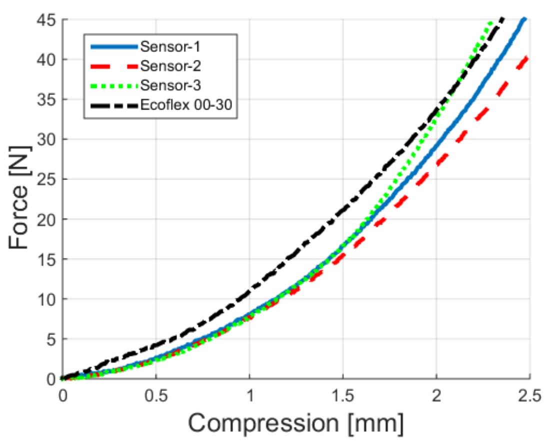

Fig. 3: Force versus compression data is obtained from three sensors and compared to a solid Ecoflex 0030 segment, indicating minimal effect on the material compliance by the embedded magnet and electronics.

circuit board. The magnet is displaced under external forces, which creates a corresponding change in the 3-D magnetic field measurement. The sensor has a pyramidal shape, which ensures that the sensor contacts the environment mostly with its tip. In addition, the magnet is embedded deep within the pyramidal shape. This location is chosen to limit the motion of the magnet under off-center forces (to ensure that the magnet translates with minimal rotation).

The sensor is fabricated using a multi-stage composite molding process as shown in Fig. 2. For embedded electronics, we print and etch a custom printed circuit board (PCB). Standard circuit components and the Hall Effect IC (Melexis MLX90363) were soldered manually. The circuit communicates with a master device using the Serial Peripheral Interface (SPI) protocol. Once programmed, the circuit sends 8-byte messages of magnetic flux measurements in three axes with 14-bit resolution in each axis. We use an Arduino control board as the master data acquisition device and send this information to MATLAB where data processing is performed.

The first step of the fabrication process is bonding the custom PCB to an acrylic plate which has been cut into the shape of the PCB but with extensions on two sides. These extensions help maintain the orientation of the PCB during molding, after which they can be snapped off. The remaining acrylic provides a rigid base to the PCB. This custom acrylic PCB is assembled with two 3-D printed molds, which also include an extruded negative of the magnet shape to create a cavity for the magnet. As silicone rubber (Smooth-On Ecoflex 0030) is cured in this mold assembly, the sensor is demolded, the magnet is placed in its place, and a layer of silicone rubber is injected in the cavity above the magnet to seal it completely within the sensor body.

A major concern in soft sensing is to ensure that the additional embedded components do not drastically modify the mechanical response of the soft body. To validate this property for our sensor design (comprising an acrylic plate, a miniature magnet, electronic components and silicone rubber substrate), we performed compressive testing of three prototypes. We compared the mechanical force-displacement response of these complete prototypes to the material response of solid silicone rubber (Ecoflex 0030) with the same geometry but without the embedded components. Our results in Fig. 3 show that material properties are similar between different batches of the sensor. We did not observe a significant change in material response due to the composite structure.

This article has been accepted for publication in a future issue of this journal, but has not been fully edited. Content may change prior to final publication. Citation information: DOI 10.1109/JSEN.2018.2814839, IEEE Sensors Journal

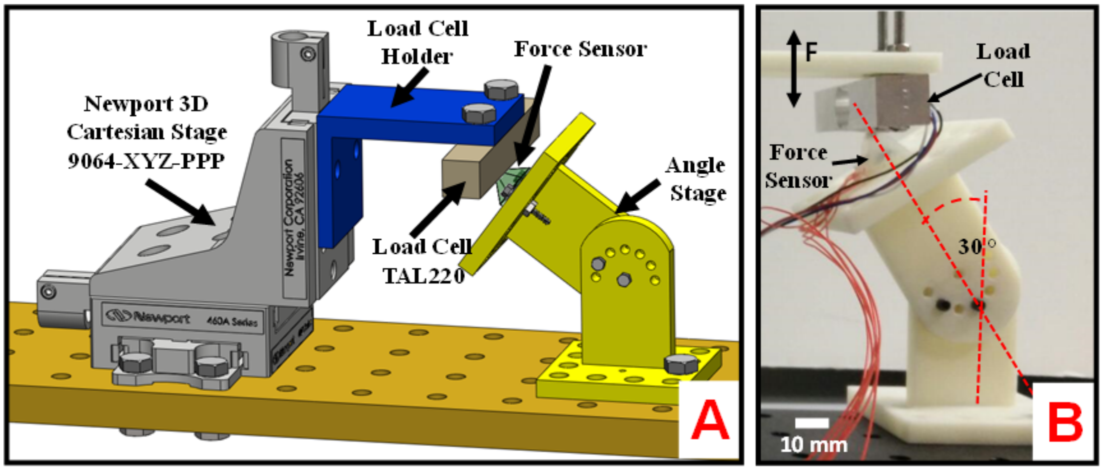

Fig. 4: Experimental setup for static loading shown as a CAD model (A) and the real system during operation (B). The force sensor placed below the load cell. The bottom stage can be rotated to a desired angle to create shear forces at a defined angle. Load generation on the sensor is achieved through lowering the load cell on the sensor by the motion stage. Thus, even though the load cell measures single axis force data, it is decoupled into normal and shear components using the angle set at the bottom stage .

III. Learning Sensor Model using a Neural Network

A multi-layer perceptron (MLP) also known as fully-connected neural (FCN) network was used to learn the function space for sensor characterization. This function space is high-dimensional and nonlinear. For instance, the soft material deformation can be described using a hyper-elastic material model such as Mooney-Rivlin or Ogden, which require multiple experimentally characterized parameters. In addition, since the relation between the magnet pose and magnetic flux is a nonlinear transformation, an analytical physics based model is intractable and a multi-physical finite element model may prove computationally expensive to operate in real-time. Thus, this work considers the use of MLPs to represent the sensor response under force loading.

Let $f_W(X_i)$ be the function that maps Hall Effect voltages to 3-D forces. The input space is the Hall Effect voltages measured by the sensor, where $\vec{X}_i = [V_x, V_y, V_z]' \in R^{3\times1}$ and the force vector corresponding to these magnetic flux values is defined as $\vec{y}_i = [F_x, F_y, F_z]' \in R^{3\times1}$. The goal of the network is to learn a set of weights W for f_W in the generic expression: $y_i = f_W(X_i)$.

A. Data Acquisition

The training data was obtained by applying known forces on the proposed soft force sensor prototypes and then measuring the corresponding Hall Effect voltage readings. The applied forces were measured using a load cell (TAL220) and corresponding amplifier circuit (Sparkfun HX711). This setup measures loads up to 10 N with errors up to 5 mN. We mount the load cell on a tri-axis Cartesian stage (Newport 9064-XYZ-PPP) as shown in Figure 4. An articulating base was designed and used to mount the sensor at desired angles with respect to the load cell, thus the force vector is decomposed into normal and shear components at known combinations. The load cell, the tri-axis stage, and the articulating base were made up of materials which do not interfere with the magnetic flux measured by the sensor.

We collected experimental data from four different sensor prototypes. The data from three sensors were used to train the neural network and the fourth sensor was used for validating the network. Four different loading configurations were considered. These include pure normal force loading (at 0°), and shear loading at angles of 30°, 45°, and 60° with respect to the sensor normal. For pure normal loading, the sensor was subjected to a maximum of 1.1 N, and for shear loading the maximum load applied was 1.5 N. These limits were chosen based on the saturation range of the Hall element and the amplifier circuit and correspond to tactile contact-level forces. Data for forces at 45° shear loading was retained only for the validation dataset and was not part of the training data. This was to see how well the trained mapping function is generalized to forces at different loading conditions.

B. Learning Approach

The technique used for learning the unknown mapping function was based on the Net2Net initialization technique [26], which performs learning in a sequential manner starting with small MLPs and then scaling the neural network up to a larger size in width and depth by using the previous smaller network as a teacher to the new larger student network. This approach avoids the usage of a very large initial network and then re-learning the entire network from scratch if the performance is not suitable. In addition, we expect this approach will help avoid overfitting and provide mapping functions that generalize well to different loading conditions and sensor prototypes. The scaling of the network is performed by initialising the student network with the weights of the teacher network and then widening or deepening it. Widening involves adding additional neurons to a layer. Deepening involves adding a new hidden layer to the network. The advantage of the method is that it ensures that the student network improves upon the teacher network.

TABLE I: MSE Loss in training during widening operation on Pyramidal Sensor

Number of Neurons in First Hidden Layer	2	4	8	16	18
MSE Loss (N^2)	0.0678	0.0325	0.0084	0.0045	0.0041

TABLE II: MSE Loss in training during deepening operation on Pyramidal Sensor

Number of Hidden Layers	1	2	3	4	5
MSE Loss (N^2)	0.0041	0.0023	$7.07\text{x}10^{-4}$	$2.45\text{x}10^{-4}$	$1.16\text{x}10^{-4}$

TABLE III: Results on the Test Dataset during widening operation on Pyramidal Sensor

Number of Neurons in First Hidden Layer	2	4	8	16	18
MAE (N)	0.23	0.13	0.092	0.053	0.052
Mean Error (N)	-0.0016	-0.0026	-0.0037	-0.0048	0.0039
σ**(N)**	0.2606	0.179	0.0917	0.0664	0.0632

TABLE IV: Results on the Test Dataset during deepening operation on Pyramidal Sensor

Number of Hidden Layers	1	2	3	4	5
MAE (N)	0.052	0.0258	0.015	0.007	0.0056
Mean Error (N)	0.0039	0.0028	0.0033	0.00094	0.00025
σ**(N)**	0.0632	0.0464	0.0262	0.0112	0.0092

C. Metrics for Evaluation

We measure the neural network performance using mean absolute error (MAE) and standard deviation (σ). Specifically, as each sensor data (X_i) is passed through the network, a prediction (p_i) is obtained and the error (e_i) is defined as the difference between this prediction and the actual force (y_i). $e_i = p_i - y_i$ where, $p_i = f_W(X_i)$. MAE and σ are calculated in standard form:

$$MAE = \frac{\sum_{i=1}^{N} e_i}{N}, \tag{1}$$

$$\sigma = \sqrt{\frac{\sum_{i=1}^{N} e_i^2}{N}}. \tag{2}$$

D. Training, Testing, and Validation

The total data points were split into training and testing datasets following the 80-20 convention. Data points obtained from the fourth sensor prototype and for 45^o loading were excluded from this dataset.

The technique used for training all the Net2Net networks utilized the following hyper parameters. All the models were trained with Adam as the optimizer and mean-squared-error (MSE) was used as the cost metric to train the network since this is a regression problem. The learning rate was scheduled with initial value being the default $1\mathrm{e}{-3}$ (for Adam optimizer). A reduction in learning rate by a factor of 10 was effected whenever the loss failed to reduce in 3 consecutive epochs. When the "Learning Rate Scheduler" function is evoked, the best weights (in terms of least loss) obtained until the function call are loaded and training is continued from there. Training was performed for 550 Epochs for each teacher network. Scaling of the network was done by widening the network first and then deepening it. Widening operation was done to a maximum of 18 neurons and then deepening operations were performed up to 5 hidden layers. The final network used for learning the sensor model contains 5-hidden layers with 18 neurons at each layer. We implemented our network models using the software package Keras [28].

E. Training Results

The MSE obtained during training is shown in Table I (for widening operation) and Table II (for deepening operation). Data from Table I indicate that the training loss converges and does not improve from 16 neurons to 18 neurons during the widening operation. This is the primary reason why the widening operations were not pursued after 18 neurons. As hidden layers are added, the training loss is almost halved for every added layer and is almost $1\mathrm{e}{-4}$ thus showing that the network is learning the function space effectively based on the training data. After adding the 5th hidden layer we concluded that further increase in depth will be prone to overfitting. However, this does not provide any insight into the capability of the network to generalize for different loading conditions and sensor prototypes. Section IV-A will demonstrate the response of the neural network for loading conditions and sensor prototypes that were not included in the training set.

F. Testing Results

Table III shows the results obtained on the test dataset during widening operations. As we scale the neurons in the first layer we see that the Mean Absolute Error (MAE) and the Standard Deviation (σ) are reduced. This decrease is very rapid initially and then slowly converges to steady state at a

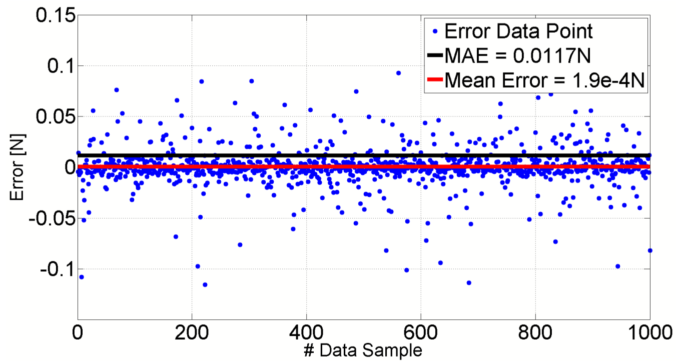

Fig. 5: Validation Dataset Error Analysis

layer width of 18 neurons. Comparing the MAE results from the 16 Neuron and 18 Neuron architectures, we see that there is negligible difference between them. This pattern is also seen in the training data and this trend shows us that further increase in the number of neurons would not provide better results. Hence widening operation was stopped at 18 Neurons and we move to performing deepening operations with 18 Neurons in each hidden unit.

Table IV shows the results when deepening operation is performed while keeping the number of neurons in each layer constant at 18 Neurons. We see that MAE and σ are halved everytime a new hidden layer is added. We stop at 5 hidden layers as adding more layers would affect the time taken for prediction during test time. At the 5th layer, we obtain a MAE of 5.6 mN and a σ of 9.2 mN which demonstrate strong prediction capability of the proposed network after both widening and deepening operations of Net2Net learning.

IV. Experimental Results

To validate the accuracy and utility of the proposed 3-D soft force sensor and neural network based modeling approach, we performed three sets of experiments. First, we applied known static and dynamic forces on the sensors and compared the outputs from the neural network with the applied forces in a validation dataset. Next, we performed a proof of concept force controlled pick and place experiment using the proposed soft triaxial force sensor mounted on the gripper of a commercial robotic manipulator to demonstrate a usage scenario where this common manipulation task greatly benefits from real-time 3-D force measurements.

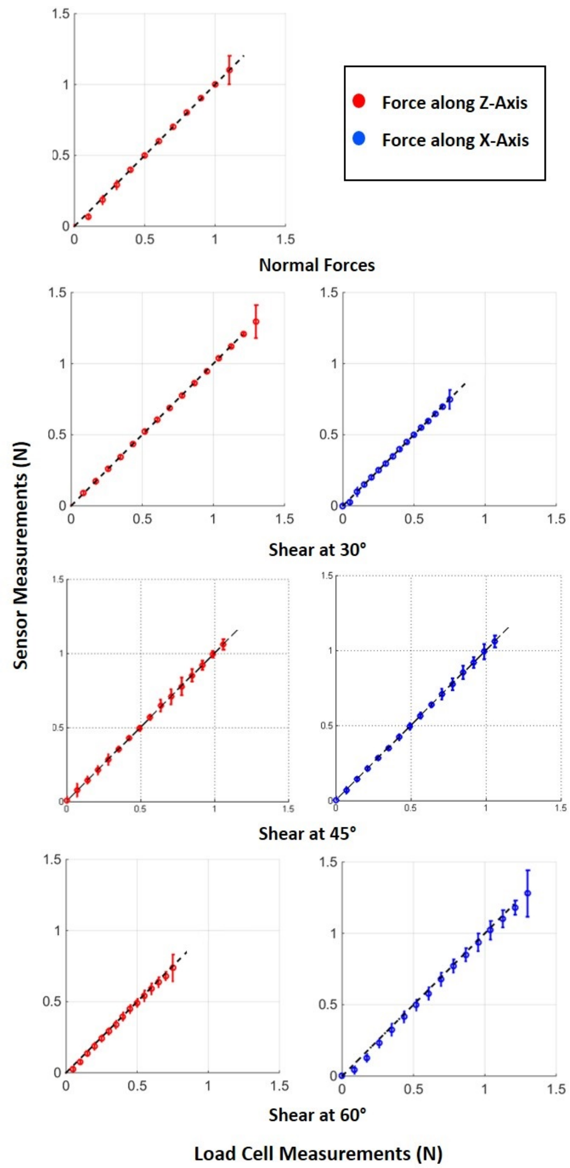

Fig. 6: Forces measured from load cell are plotted on X-axis whereas forces measured from the soft force sensor are plotted on Y-axis. The circles represent the mean measurement value and a standard deviation for each point is also provided. The top row presents the Normal Forces case. The second, third, and fourth rows represent 30, 45 and 60 degree cases, respectively. Since the shear forces were applied in the XZ plane, we omit forces along Y-axis and in Normal Force case we omit forces along both X and Y axes, which remain close to zero.

A. Static Validation Results

As previously discussed, the data obtained from the fourth sensor was not included in the training set and it was reserved for validation. The final neural network with 5 hidden layers was used to predict the forces for this sensor, and 1000 randomly sampled error points are shown in Figure 5. Figure 6 displays the actual forces (on the horizontal axis of these curves) that were applied on the sensor for pure normal loading, and shear (plus normal) loading at 30°, 45°, and 60°, all about the XZ plane and with the corresponding forces measured by the sensor using the neural network model (shown on the vertical axis). Only the relevant forces which were subject to change are plotted in the figure (i.e. the shear measurements in Y-axis remain at zero and are not shown). We see that the actual to measured force curve closely follows the expected diagonal line with a slope of 1, thus showing that the applied forces are measured accurately by the sensor using the proposed neural network model. We also see that the deviation of the measurements from actual forces is very low at low forces and more pronounced at higher loads. This could be due to the Hall element approaching the saturation limit and reducing its linearity between voltage to magnetic field

This article has been accepted for publication in a future issue of this journal, but has not been fully edited. Content may change prior to final publication. Citation information: DOI 10.1109/JSEN.2018.2814839, IEEE Sensors Journal

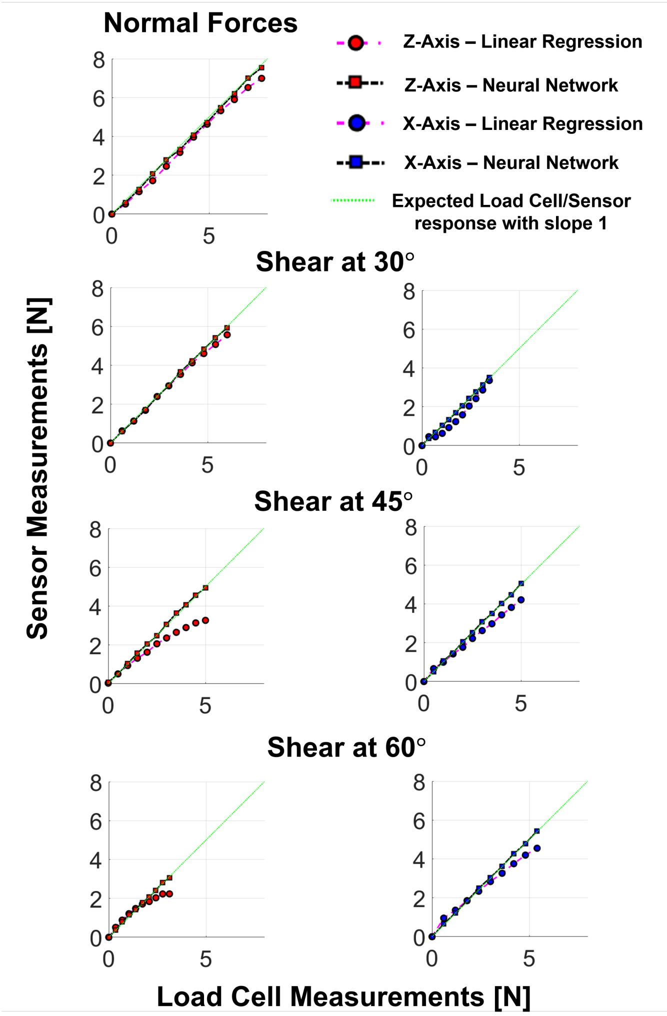

Fig. 7: Pyramidal sensor with Dragonskin 30 as the soft substrate. The comparison of linear regression (dashed magenta lines with circle markers) and trained neural network forces (dash-dot black lines with square markers) are overlaid. Forces measured from load cell are plotted on the X-axis whereas forces measured from the soft force sensor are plotted on the Y-axis. The top row presents pure normal loading. The second, third, and fourth rows represent 30, 45, and 60 degree loading cases, respectively. Since the shear forces were applied in the XZ plane, we omit forces along Y-axis and in Normal Force case we omit forces along both X and Y axes.

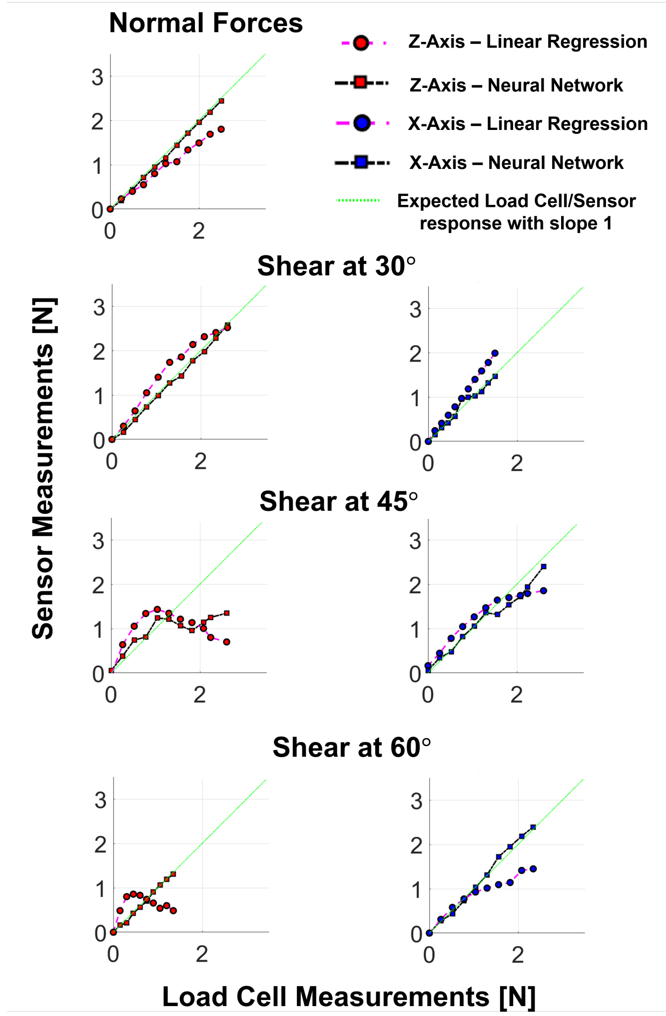

Fig. 8: Rectangular sensor with Ecoflex 0030 as the soft substrate. The comparison of linear regression (dashed magenta lines with circle markers) and trained neural network forces (dash-dot black lines with square markers) are overlaid. Forces measured from load cell are plotted on the X-axis whereas forces measured from the soft force sensor are plotted on the Y-axis. The top row presents pure normal loading. The second, third, and fourth rows represent 30, 45, and 60 degree loading cases, respectively. Since the shear forces were applied in the XZ plane, we omit forces along Y-axis and in Normal Force case we omit forces along both X and Y axes.

values. A MAE of 11.7 mN was obtained on the magnitude of the forces on this dataset. Also, the FCN network is able to accurately measure the forces for shear loading at 45°, (a loading condition for which it was not trained and on a sensor prototype which was not included in training). From these experiments, we conclude that the network is able to generalize very well on new sensors and loading conditions. The time required for predicting forces during validation for each input vector (three Hall voltages) to the neural network was 0.34 msec and thus the FCN does not introduce time delay into the sensing system during real-time operation.

It is true that complex modeling schemes are usually undesirable and thus, we need to justify our choice of using a neural network model to calculate the 3-D forces from Hall voltage signals. To show neural network modeling is useful for soft force sensors with complex shapes and hyper elastic materials, we compared sensor measurements from the neural network with a simpler calibration approach, linear regression. The results are shown in Figure 7. Sensed forces from the FCN outperformed linear regression results in all cases. An MAE of 1.23 N was observed on the validation data when trained with linear regression. The MAE from the the neural network on the same dataset was 0.3014 N. In the 45° case, which was not included in the training set for either approach, linear regression significantly underperformed as well.

The sensor data shown in Figure 7 is obtained from a sensor made with Smooth-On Dragonskin 30 as opposed to Ecoflex 0030. Since Dragonskin 30 is a stiffer material, a cor-

This article has been accepted for publication in a future issue of this journal, but has not been fully edited. Content may change prior to final publication. Citation information: DOI 10.1109/JSEN.2018.2814839, IEEE Sensors Journal

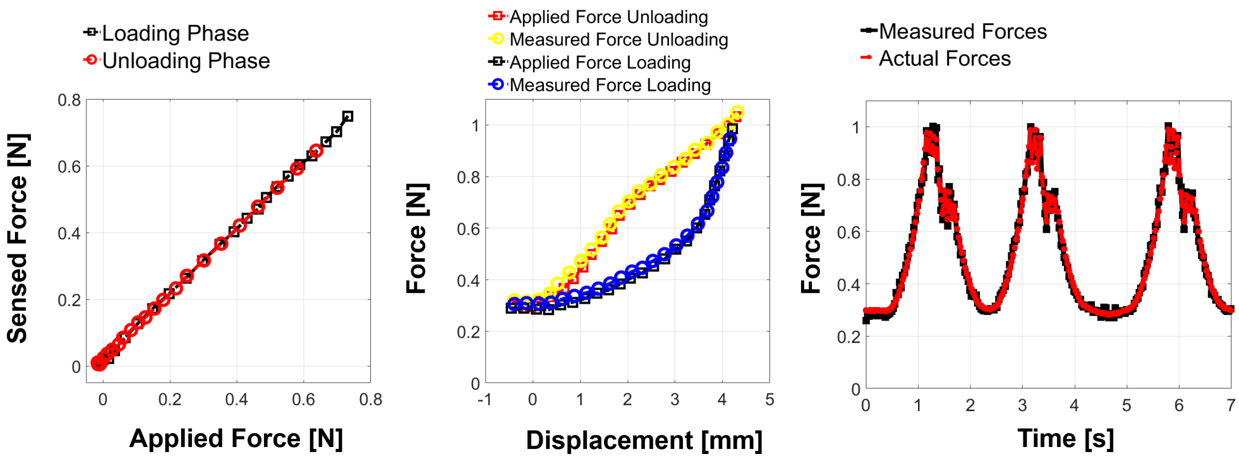

Fig. 9: Dynamic testing results indicate that applied and measured forces follow a 1-1 diagonal (left). Hysteresis of loading and unloading for the applied and measured force-displacement data are in agreement (middle). The tracking of applied and measured forces during dynamic loading overlap in time axis (7 seconds shown from the 150-second experiment) (right).

responding increase in the measured force range is observed. Our results indicate that the same neural network calibration approach adjusts well to different material types with the same sensor shape.

In addition, a justification is needed for our choice of using a pyramid shape for the sensor since it is more complex than a simple rectangular block design. To this end, we made the same set of experiments on a rectangular sensor design made from Ecoflex 0030 and kept the distance between the magnet and the IC surface same as in the pyramidal shape sensor and following the same calibration routine. Our experimental results are shown in Figure 8. Just as with the Dragonskin 30 pyramid design, forces obtained from neural network are more accurate as opposed to linear regression where MAE on validation dataset was 0.1110 N and 0.2827 N, respectively. However, small deviations in 30°, 60° and a large deviation in z-axis measurement in 45° suggests rectangular shape to be undesirable for accurate force measurements. We attribute these deviations to free magnet rotations when pushed at an angle on the rectangular surface. The pyramid shape, on the other hand, allows us to position the magnet near the centroid and reduce undesired rotations of the magnet, enabling repeatable and accurate force measurements.

B. Dynamic Validation Results

Dynamic loading experiments were performed using an Instron Electroplus-e1000 Linear-Torsion force testing instrument at WPI Biomedical Engineering Department. Only normal compressive forces were applied on the sensor and the frequency of the applied forces was set at 0.6 Hz (limited by the speed of the instrument) and the forces applied were between 0.3 N and 1.0 N as shown in Figure 9. The sensor was pre-compressed using a force of 0.3 N to eliminate any potential shifting of the sensor during the experiments. The application of dynamic forces on silicone rubber results in hysteresis due to viscoelastic effects (i.e. the deflection of the material differs for the same force during loading and unloading). The hysteresis plot is shown in Figure 9-Middle Panel. This curve indicates that the measured forces follow the actual force closely. In other words, the proposed sensor is able to map the effect of hysteresis very well and provide a measure of dynamic forces accurately. Figure 9-Right Panel shows the time response during a representative dynamic loading experiment, where the sensor output tracks the applied dynamic forces. The accuracy of dynamic force measurements is better inferred from Figure 9-Left Panel, which shows measured force with respect to corresponding applied force. Here we see that the relationship between the measured and applied forces follows a line with a slope equal to 1.0 with minimal variation.

C. Force Controlled Pick and Place Case Study

The proposed force sensor can be used to grasp soft or delicate objects with manipulators that are not designed to handle such objects. To demonstrate this application, we perform a pick and place experiment with the Jaco arm (Kinova robotics, Boisbriand, QC, Canada) manipulating an egg. The arm is a 6-degree-of-freedom (DOF) manipulator with a 3-finger gripper. With the proposed soft tri-axial force sensor we are able to perform force control and thus the manipulator is able to transport the egg from one location to another without breaking it.

The arm was programmed to perform the pick and place task between two known locations on a tabletop. The goal is for the arm to sense the forces applied on the egg in real time to establish and maintain a gentle grip and release the egg when it touches the table top at the destination. The software to operate the arm was developed using Robot Operating system (ROS) [31]. The manipulator arm was configured to follow a trajectory in multiple phases. The corresponding forces measured in the phases are shown in Figure 10. Here, the sensor is placed on the finger pad, where normal contact forces coincide with the z-axis (local normal) of the sensor and gravity is along the y-axis (local shear). There are no expected forces along the x-axis, which is reflected in the measurements.

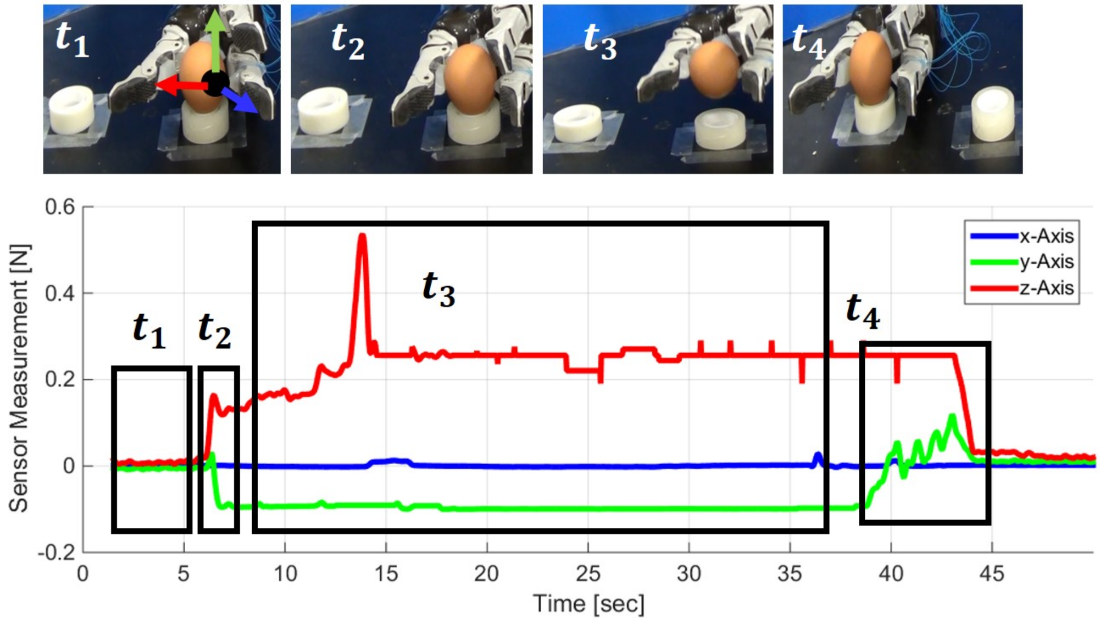

Fig. 10: Significant time intervals from the grasp experiment are shown. At t_1 robot is at its initial state and no force is measured on the sensor. Shear force and normal force are detected as fingers get in contact with the object during t_2. The interval t_3 represents the movement of the object from initial point to the target point. The peak in this interval is due to stabilization of the egg between two fingers. Finally the object is released by detecting the change in y-axis force in interval t_4. A coordinate frame attached to the first snapshot at t_1 represents the measurement axes of the force sensor.

The gap in the gripper when fingers are fully closed was bigger than the size of the egg. Hence, the gripper fingers were padded with a silicone rubber layer in order to reduce this gap. The weight of the egg was 50 g. The arm could lift the egg without any damage following a simple force-control process as shown as snapshots in Figure 10. The four phases during this task are defined as follows:

Gripper Closing Phase: Shown by the period t_1 in Figure 10, here the gripper is at the initial pose and the fingers start closing. All forces remain at 0 N throughout this period, taking about 6 seconds before the fingers make contact with the egg.

Grasping and Lifting Phase: Shown by the period t_2 in Figure 10, here the gripper initiates contact with the egg as seen by the increase in F_Z. The fingers continue closing until a predefined threshold is reached to produce a normal grasping force between contact surfaces to hold on to the object due to friction, with negligible deformation. The value of the safe limit was determined through prior trials to be 0.15 N to 0.35 N (as measured by the force sensor) for the egg. After grasping the object, the arm starts lifting up the egg at around 7 seconds. In this phase, the force sensor experiences an increase in the shear force F_Y due to gravity.

Relocating Phase: Shown by the period t_3 in Figure 10, here the arm moves the gripper along with the egg over to a destination location while keeping the gripper position 10 cm above the desk level. Slight disturbances are seen in this time period which could be attributed to a shaky movement of the Jaco arm. The short pulse in this phase at 14 seconds coincides with a slight shift in the position of the egg between the fingers.

Placing Phase: Shown by the period t_4 in Figure 10, the gripper moves down towards the table. As the egg makes contact with the table top, the shear force decreases. This decrease in shear force allows the arm to recognise that the egg has been placed at the destination spot. At this time, the Jaco arm opens its grip to release the egg and the arm goes back to the starting position.

The sensing of the shear forces while placing an object helps the manipulator to sense that the object has made contact with the ground surface and allow it to place the object safely and gently at the destination spot without dropping the object or strongly hitting the ground surface.

V. Conclusion and Future Work

In this paper we described the design, fabrication, characterization, and experimental validation of a Hall effect based 3-D soft force sensor in a pyramid shaped soft elastomer matrix. We trained a fully-connected neural network for characterization and mapping of measured voltages to 3-D forces. We show that the resulting mapping generalizes well for sensors and loading conditions that are not part of the training dataset. Our experimental results show that the proposed sensor is highly accurate and it can measure forces in normal and shear directions within a range of 0 N to 1.1 N and ±1.5 N with an error of 2% and 2.2% of the full scale reading in normal and shear, respectively. The bandwidth of the Melexis sensor IC can work up to 400 Hz. Dynamic loading experiments indicate that the sensor is able to accurately follow dynamic forces applied at 0.6 Hz despite the hysteresis exhibited by the material.

TABLE V: Comparison of commercial and published force sensors along with the Pyramidal Ecoflex 0030 sensor presented in this paper along important properties of size, sampling rate, hysteresis, measured force axes, range and sensitivity.

Sensor Name	**L×W×H (mm)**	**Sampling Rate**	**Hysteresis**	**Decoupled Force/Torque Axes**	**Range (N)**	**Sensitivity**
Tekscan (A101)	15×7×0.2	200 kHz [1]	4.5% FS	1	44	No data provided
Single Tact Sensor	58×8×0.35	1000 Hz	4% FS	1	10	20 mN
OMD-10-SE-10N	15×11×10	1000 Hz	2% FS	3	$Fz = 10$ $Fx = \pm 2.5$ $Fy = \pm 2.5$	2.5 mN
Embedded Microfluidic Channels [9]	50×60×7	100 Hz [2]	Negligible [3]	3	$Fz = 6$ $Fx = \pm 1$ $Fy = \pm 1$	10 mN
Tomo et al. [22]	55×55×8	100 Hz	No data provided [4]	3	$Fz = 15$ $Fx = \pm 6$ $Fy = \pm 6$	No data provided
Nie et al. [29]	Diameter: 60×11	400 Hz	No data provided	4	$Fz = 40$ $Fx = 15$ $Fy = 15$ $Tz = 0.8$	10 mN
Liu et al. [30]	Diameter: 20×8	5 kHz	No data provided	3	$Fz = 0.5$ $Fx = 0.5$ $Fy = 0.5$	10 mN
This Work: Pyramidal Ecoflex 0030	12×12×8	400 Hz	Negligible [5]	3	$Fz = 1.1$ $Fx = \pm 1.5$ $Fy = \pm 1.5$	5 mN

[1]The value is based on the response time of the piezoresistive material. The bandwidth may vary for different uses.
[2]Reported sampling rate.
[3]The material will exhibit viscoelastic properties.
[4]The material will exhibit viscoelastic properties.
[5]The pyramid sensor exhibits negligible hysteresis for force measurements. A higher hysteresis of 24% is observed in force-displacement response. This behaviour is due to the viscoelastic nature of the material.

We present a comparison of the pyramidal Ecoflex 0030 sensor with commercially available and published force sensor designs in Table V. Hysteresis in piezoelectric and capacitive commercially available sensors seems negligible but our findings suggest viscoelasticity of soft materials adds significant hysteresis and we expect other works that use similar materials to exhibit hysteresis effects. In most cases the range of the sensor can be adjusted by picking different soft materials or adjusting the gains of the amplifier attached to the sensor. The pyramidal Ecoflex 0030 sensor is quite sensitive, measuring forces as small as 5 mN (error range of the load cell used for calibration) within a suitable range of 0-1 N for tactile applications. In Table V, Single Tact Sensor and embedded microfluidic channel based sensor design stand out as high sensitivity sensors within their maximum force range. Single Tact Sensor, however is only capable of measurements in a single dimension. As for sensitivity the Ecoflex 0030 Pyramid sensor (5 mN) is only outperformed by the commercial OMD-10 sensor (2.5 mN). In terms of package size the Ecoflex 0030 Pyramid sensor has a volume of 380 mm^3. Sensors having a smaller volume are Tekscan and Single Tact Sensor, which only provide normal force measurements. This volume difference is expected since both sensors are fabricated on a thin sheet and do not have soft substrates over them. Overall, we conclude that the pyramid sensor shape, magnetic field measurements, and a soft substrate as the force measurement medium provides a good combination of size, measured axes, and sensitivity.

A force controlled pick and place experiment was performed on an egg using the force sensor mounted on a Kinova Jaco arm. We show that the sensor provides stable output force data in real-time and we can use both shear and normal force data to successfully perform fragile object manipulation.

Future work will focus on the combination of multiple sensor units in an array. These arrays of force sensors will help monitor accurate distributed force measurements in 3-D. More work is planned to further study the effect of the shape of the sensor and the location of the magnet within this shape. Usage of the sensor in tasks such as walking gait and balance analysis and haptic feedback will also be explored.

ACKNOWLEDGEMENTS

The authors would like to thank Joshua R. Gershlak from the Biomedical Engineering Department at WPI for his valuable assistance on the dynamic testing of the sensor.

REFERENCES

[1] R. S. Dahiya, G. Metta, M. Valle, and G. Sandini, "Tactile sensing—from humans to humanoids," *IEEE Transactions on Robotics*, vol. 26, no. 1, pp. 1–20, 2010.
[2] H. R. Nicholls and M. H. Lee, "A survey of robot tactile sensing technology," *The International Journal of Robotics Research*, vol. 8, no. 3, pp. 3–30, 1989.
[3] H. Yousef, M. Boukallel, and K. Althoefer, "Tactile sensing for dexterous in-hand manipulation in robotics—a review," *Sensors and Actuators A: Physical*, vol. 167, no. 2, pp. 171 – 187, 2011. Solid-State Sensors, Actuators and Microsystems Workshop.

[4] J. J. Clark, "A magnetic field based compliance matching sensor for high resolution, high compliance tactile sensing," in *Robotics and Automation, 1988. Proceedings., 1988 IEEE International Conference on*, pp. 772–777 vol.2, Apr 1988.

[5] R. B. Katragadda and Y. Xu, "A novel intelligent textile technology based on silicon flexible skins," *Sensors and Actuators A: Physical*, vol. 143, no. 1, pp. 169–174, 2008.

[6] K. Noda, K. Hoshino, K. Matsumoto, and I. Shimoyama, "A shear stress sensor for tactile sensing with the piezoresistive cantilever standing in elastic material," *Sensors and Actuators A: physical*, vol. 127, no. 2, pp. 295–301, 2006.

[7] K. Kim, K. R. Lee, W. H. Kim, K.-B. Park, T.-H. Kim, J.-S. Kim, and J. J. Pak, "Polymer-based flexible tactile sensor up to 32× 32 arrays integrated with interconnection terminals," *Sensors and Actuators A: Physical*, vol. 156, no. 2, pp. 284–291, 2009.

[8] M. Sohgawa, T. Mima, H. Onishi, T. Kanashima, M. Okuyama, K. Yamashita, M. Noda, M. Higuchi, and H. Noma, "Tactle array sensor with inclined chromium/silicon piezoresistive cantilevers embedded in elastomer," in *TRANSDUCERS 2009 - 2009 International Solid-State Sensors, Actuators and Microsystems Conference*, pp. 284–287, June 2009.

[9] D. M. Vogt, Y. L. Park, and R. J. Wood, "Design and characterization of a soft multi-axis force sensor using embedded microfluidic channels," *IEEE Sensors Journal*, vol. 13, pp. 4056–4064, Oct 2013.

[10] M. Khondoker and D. Sameoto, "Fabrication methods and applications of microstructured gallium based liquid metal alloys," *Smart Materials and Structures*, vol. 25, no. 9, p. 093001, 2016.

[11] D. J. Lipomi, M. Vosgueritchian, B. C. Tee, S. L. Hellstrom, J. A. Lee, C. H. Fox, and Z. Bao, "Skin-like pressure and strain sensors based on transparent elastic films of carbon nanotubes," *Nature nanotechnology*, vol. 6, no. 12, pp. 788–792, 2011.

[12] L. Viry, A. Levi, M. Totaro, A. Mondini, V. Mattoli, B. Mazzolai, and L. Beccai, "Flexible three-axial force sensor for soft and highly sensitive artificial touch," *Advanced materials*, vol. 26, no. 17, pp. 2659–2664, 2014.

[13] Y. Yang and Y. Chen, "Innovative design of embedded pressure and position sensors for soft actuators," *IEEE Robotics and Automation Letters*, vol. 3, pp. 656–663, April 2018.

[14] Y. Tenzer, L. P. Jentoft, and R. D. Howe, "The feel of mems barometers: Inexpensive and easily customized tactile array sensors," *IEEE Robotics & Automation Magazine*, vol. 21, no. 3, pp. 89–95, 2014.

[15] J. Yi, X. Zhu, L. Shen, B. Sun, and L. Jiang, *An Orthogonal Curvature Fiber Bragg Grating Sensor Array for Shape Reconstruction*, pp. 25–31. Berlin, Heidelberg: Springer Berlin Heidelberg, 2010.

[16] S. Youssefian, N. Rahbar, and E. Torres-Jara, "Contact behavior of soft spherical tactile sensors," *IEEE Sensors Journal*, vol. 14, pp. 1435–1442, May 2014.

[17] C. Cho and Y. Ryuh, "Fabrication of flexible tactile force sensor using conductive ink and silicon elastomer," *Sensors and Actuators A: Physical*, vol. 237, pp. 72–80, 2016.

[18] S. Ozel, N. A. Keskin, D. Khea, and C. D. Onal, "A precise embedded curvature sensor module for soft-bodied robots," 2015.

[19] M. Luo, Y. Pan, E. H. Skorina, W. Tao, F. Chen, S. Ozel, and C. D. Onal, "Slithering towards autonomy: a self-contained soft robotic snake platform with integrated curvature sensing.," *Bioinspiration & biomimetics*, vol. 10 5, p. 055001, 2015.

[20] C. Ledermann, S. Wirges, D. Oertel, M. Mende, and H. Woern, "Tactile sensor on a magnetic basis using novel 3d hall sensor-first prototypes and results," in *Intelligent Engineering Systems (INES), 2013 IEEE 17th International Conference on*, pp. 55–60, IEEE, 2013.

[21] L. Jamone, G. Metta, F. Nori, and G. Sandini, "James: A humanoid robot acting over an unstructured world," in *Humanoid Robots, 2006 6th IEEE-RAS International Conference on*, pp. 143–150, IEEE, 2006.

[22] T. P. Tomo, S. Somlor, A. Schmitz, L. Jamone, W. Huang, H. Kristanto, and S. Sugano, "Design and characterization of a three-axis hall effect-based soft skin sensor," *Sensors*, vol. 16, no. 4, p. 491, 2016.

[23] E. Torres-Jara, I. Vasilescu, and R. Coral, "A soft touch: Compliant tactile sensors for sensitive manipulation," 2006.

[24] T. P. Tomo, W. K. Wong, A. Schmitz, H. Kristanto, S. Somlor, J. Hwang, and S. Sugano, "Snr modeling and material dependency test of a low-cost and simple to fabricate 3d force sensor for soft robotics," in *System Integration (SII), 2016 IEEE/SICE International Symposium on*, pp. 428–433, IEEE, 2016.

[25] J. Gafford, F. Doshi-Velez, R. Wood, and C. Walsh, "Machine learning approaches to environmental disturbance rejection in multi-axis opto-electronic force sensors," *Sensors and Actuators A: Physical*, vol. 248, pp. 78–87, 2016.

[26] T. Chen, I. Goodfellow, and J. Shlens, "Net2net: Accelerating learning via knowledge transfer," *arXiv preprint arXiv:1511.05641*, 2015.

[27] C. Li, P. M. Wu, S. Lee, A. Gorton, M. J. Schulz, and C. H. Ahn, "Flexible dome and bump shape piezoelectric tactile sensors using pvdf-trfe copolymer," *Journal of Microelectromechanical Systems*, vol. 17, pp. 334–341, April 2008.

[28] F. Chollet, "Keras." https://github.com/fchollet/keras, 2015.

[29] Q. Nie and F. C. Sup, "A soft four degree-of-freedom load cell based on the hall effect," *IEEE Sensors Journal*, vol. 17, pp. 7355–7363, Nov 2017.

[30] Y. Liu, H. Han, T. Liu, J. Yi, Q. Li, and Y. Inoue, "A novel tactile sensor with electromagnetic induction and its application on stick-slip interaction detection," *Sensors*, vol. 16, no. 4, 2016.

[31] M. Quigley, K. Conley, B. Gerkey, J. Faust, T. Foote, J. Leibs, R. Wheeler, and A. Y. Ng, "Ros: an open-source robot operating system," in *ICRA workshop on open source software*, vol. 3, p. 5, Kobe, 2009.